AMOC Stabilization under the Interaction with Tipping Polar Ice Sheets

Sacha Sinet[1,1], Henk A. Dijkstra[2,2], and Anna S. von der Heydt[1,1]

[1]Institute for Marine and Atmospheric research Utrecht, Utrecht University
[2]Institute for Marine and Atmospheric research Utrecht

November 30, 2022

Abstract

Several large-scale components of the climate system may undergo a rapid transition as critical conditions are exceeded. These tipping elements are also dynamically coupled, allowing for a global domino effect under global warming. Here we focus on such cascading events involving the Greenland Ice Sheet (GIS), the West Antarctica Ice Sheet (WAIS) and the Atlantic Meridional Overturning Circulation (AMOC). Using a conceptual model, we study the combined tipping behavior due to three dominant feedbacks: the marine ice sheet instability for the WAIS, the height-surface mass balance feedback for the GIS and the salt-advection feedback for the AMOC. We show that, in a realistic parameter range of the model, a tipping of the WAIS can inhibit cascading events by preserving the AMOC stability.

AMOC Stabilization under the Interaction with Tipping Polar Ice Sheets

S. Sinet[1,2], A. S. von der Heydt[1,2], and H. A. Dijkstra[1,2]

[1]Institute for Marine and Atmospheric research Utrecht, Department of Physics, Utrecht University, Utrecht, The Netherlands
[2]Center for Complex Systems Studies, Department of Physics, Utrecht University, Utrecht, The Netherlands

Key Points:

- A conceptual model of interacting AMOC, GIS and WAIS is presented
- Interactions between these tipping elements strongly modifies the stability of the whole system
- A collapse of the WAIS can prevent tipping of the AMOC

Corresponding author: Sacha Sinet, s.a.m.sinet@uu.nl

Abstract

Several large-scale components of the climate system may undergo a rapid transition as critical conditions are exceeded. These tipping elements are also dynamically coupled, allowing for a global domino effect under global warming. Here we focus on such cascading events involving the Greenland Ice Sheet (GIS), the West Antarctica Ice Sheet (WAIS) and the Atlantic Meridional Overturning Circulation (AMOC). Using a conceptual model, we study the combined tipping behavior due to three dominant feedbacks: the marine ice sheet instability for the WAIS, the height-surface mass balance feedback for the GIS and the salt-advection feedback for the AMOC. We show that, in a realistic parameter range of the model, a tipping of the WAIS can inhibit cascading events by preserving the AMOC stability.

Plain Language Summary

In the climate system, the interaction of specific components known as tipping elements are thought to be able to induce a global domino effect, or cascading tipping. In this study, we present a conceptual model containing the most strongly interacting components, namely the Atlantic Meridional Overturning Circulation (AMOC), the Greenland Ice Sheet and the West Antarctica Ice Sheet. We find that the stability of this system as a whole is strongly modified when interactions are included. Especially, while a Greenland Ice Sheet collapse destabilizes the AMOC, the model shows that a collapse of the West Antarctica Ice Sheet might prevent a global cascading event by stabilizing the AMOC.

1 Introduction

Global warming is one of the main threats to the stability of the present-day climate system. Under this warming, specific climate system components might change abruptly when certain critical thresholds are exceeded. Examples of such tipping elements (Lenton et al., 2008) are the Greenland Ice Sheet (GIS), the Atlantic Meridional Overturning Circulation (AMOC), the West Antarctic Ice Sheet (WAIS) and the Amazon rainforest. A thorough understanding of the mechanisms and impact of tipping behavior in these subsystems is fundamental in assessing the risks of climate change.

Tipping elements are also strongly interacting, for example the polar ice sheets and the ocean circulation, and hence tipping in one subsystem (the leading system) may lead to tipping in another (the following system), in a so-called tipping cascade (Dekker et al., 2018). This rises the possibility of domino effects, causing the climate system to collapse while the threshold of one subsystem only has been crossed (Klose et al., 2021). However, the collapse of one subsystem may also stabilize other tipping elements and hence might be beneficial for the stability of the whole climate system.

Using expert elicitation, Kriegler et al. (2009) qualitatively assessed the risk of such cascading events in a context of global warming. In a more quantitative assessment Wunderling et al. (2021) studied the interactions between tipping of the GIS, the AMOC, the WAIS and the Amazon rainforest using a highly idealized model of coupled dynamical systems, each capturing the tipping through back-to-back saddle-node bifurcations. Here, the GIS, AMOC and WAIS stood out as the protagonists of a potential large-scale cascading. However, the Wunderling et al. (2021) approach lacks a connection to the underlying physical processes, and their interactions.

The aim of this study is to couple physically motivated conceptual models of the three tipping elements. Within a new coupled model, we study similar issues as Wunderling et al. (2021), where the GIS and AMOC were described respectively as potential initiator and mediator of cascading, while the role of the WAIS was less certain. We focus on

the conditions under which cascading can occur or not, and especially on regimes in which the AMOC can remain stable when interacting with tipping polar ice sheets under global warming.

2 Modeling coupled tipping elements

A conceptual inter-hemispheric model composed of the GIS, the AMOC and the WAIS subsystems is presented in Fig. 1. The individual model components and their coupling are described in the below paragraphs.

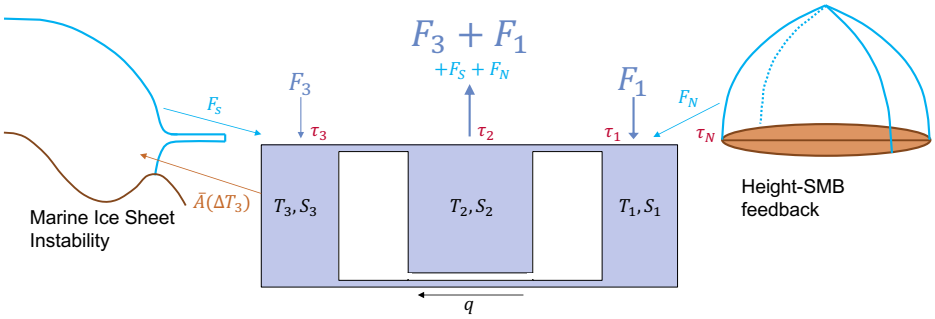

Figure 1. *Representation of the coupled model. The WAIS is represented by a single marine ice sheet in the Antarctic region. The AMOC is depicted by three boxes for the southern (under 30° S), tropical (30° S to 30° N) and northern (above 30° N) Atlantic Ocean, each one coming with their own temperatures and salinities, forced by precipitation fluxes $F_{1,3}$ and background temperatures $\tau_{1,2,3}$. The GIS is represented by a radially symmetric ice dome in the Arctic region. Both ice sheets interact with the ocean through meltwater fluxes $F_{N,S}$, and the southern Atlantic Ocean temperature T_3 interacts with the WAIS through the depth integrated ice viscosity parameter $\bar{A}(\Delta T_3)$.*

2.1 The GIS

Over the last decades, satellite measurements have revealed a significant acceleration of ice loss of the GIS (The IMBIE Team, 2020), where the decreasing surface mass balance (SMB) plays a crucial role (Enderlin et al., 2014; Goelzer et al., 2013). A critical global mean surface temperature increase threshold of $0.8 - 3.2$ °C has been suggested based on models (Robinson et al., 2012; Ridley et al., 2009; Irvalı et al., 2020), above which the GIS would be committed to melting. An important mechanism to destabilize an ice cap is the height-SMB feedback (Levermann & Winkelmann, 2016), according to which the thinning of an ice mass enhances melting as its surface reaches lower altitudes, associated with higher temperatures. Based on early warning signals, Boers and Rypdal (2021) claim that the height-SMB feedback might already have brought the GIS close to a tipping point.

To represent the GIS, we consider an isothermal ice sheet lying on a fixed bedrock (Greve & Blatter, 2009). The evolution of the ice thickness is given by the contribution of the transport inside the ice dome involving the ice flux, along with the SMB. The problem is simplified by using the shallow-ice approximation and considering a radially symmetric ice cap resting on a flat circular bed at sea level, with a no-ice condition at the boundary. The height-dependent SMB is defined using the precipitation rate and equi-

librium line altitude, which depend on the regional temperature anomaly $\Delta\tau_N$ with respect to the present-day annual mean value.

For the parameters chosen, the present-day GIS tips to an ice-free state (due to a saddle-node bifurcation) for warming values $\Delta\tau_{\mathrm{N}} > \Delta\tau_{\mathrm{N,c}} \approx 1.2°\mathrm{C}$, consistent with the low end previsions by Robinson et al. (2012). Finally, ice loss is converted to a meltwater flux F_N directly inserted in the northern Atlantic box. More details about the GIS model are provided in section S1 of the SI.

2.2 The AMOC

From long-term observations of sea surface temperature, it has been suggested (Caesar et al., 2018, 2021) that a slowing down of the AMOC has occurred over the last century. Global warming and associated changes in the hydrological cycle are overal destabilizing (Bakker et al., 2016) due to the salt-advection feedback. A tipping point ranging from 3.5 to 6 degrees of global warming is suggested in the literature (Schellnhuber et al., 2016; Lenton et al., 2008), although with high uncertainty. Also, an increased freshwater input in the deep water formation region, caused by GIS melting, is destabilizing (Jackson & Wood, 2018). Based on global climate models, Jackson and Wood (2018) have suggested a critical extra freshwater input of about 0.1 Sv, corresponding to the high end of that associated with a GIS decay (Lenaerts et al., 2015). The impact of freshwater input in the southern region, however, remains uncertain as there are numerous competing feedbacks (Swingedouw et al., 2008), but seems to be overall stabilizing. Recently, based again on early warning indicators, Boers (2021) claims that the AMOC is close to tipping.

For the AMOC, we use the three-box model of Rooth (Rooth, 1982; Scott et al., 1999; Lucarini & Stone, 2005), describing the AMOC driven by the pole-to-pole density difference. The first box represents the northern Atlantic Ocean, the second the tropical region and the third the southern Atlantic Ocean. Temperatures and salinities are changed through advective transport due to the AMOC strength q, defined positive for a present-day, northern sinking configuration. The temperature $T_{1,2,3}$ of each box is relaxed to a background temperature $\tau_{1,2,3}$, at a relaxation timescale of about 25 years. Salinities $S_{1,2,3}$ are forced by surface freshwater fluxes $F_{1,3,N,S}$, including precipitation and meltwater input at the poles, compensated by evaporation in the tropics (see Fig 1), yielding conservation of total salt content for the Atlantic Ocean. More details about the AMOC model are provided in the section S2 of the SI.

The stability of the Rooth model in a northern sinking state under varying freshwater or temperature forcing has already been investigated (Scott et al., 1999; Lucarini & Stone, 2005). On one hand, at a total freshwater input in the northern box of $F_{1,c} = 0.86$ Sv, the model undergoes a subcritical Hopf bifurcation above which only the southern sinking state remains stable, while increasing the freshwater input in the southern box strengthens the circulation. On the other hand, increasing the inter-hemispheric forcing temperature asymmetry $\tau_1 - \tau_3$ weakens the circulation. In both cases however, the associated critical values will be highly rate dependent, which will be discussed in the section 3.

2.3 The WAIS

The WAIS has seen unprecedented ice loss over the last decades (The IMBIE Team, 2018), with ocean warming being the main driver (Shepherd et al., 2004; Joughin et al., 2014; Favier et al., 2019). The increased loss is likely due to the fact that a dominant part of the WAIS ice mass is grounded under sea level, making it subject to dynamical instabilities known as the marine ice sheet instability (MISI) (Weertman, 1974; Schoof, 2007; Mulder et al., 2018). In the Amundsen sea sector, the MISI might already be ini-

tiated (Favier et al., 2014; Rignot et al., 2014), with potentially dramatic consequences for the WAIS (Feldmann & Levermann, 2015) and for the whole Antarctic continent (Garbe et al., 2020).

We consider the WAIS as one single marine ice sheet (Schoof, 2007) under depth-integrated shallow-shelf approximation, represented by a rapidly sliding, two-dimensional and symmetric marine ice sheet. A floating ice shelve is included as boundary condition at the grounding line, such that the position of the grounding line can be tracked. We consider the SMB constant and uniform, ignoring any melting contribution, as we expect dynamical ice loss to dominate when the MISI occurs. The bifurcation structure of this model with respect to the depth-integrated ice viscosity parameter $\bar{A}$ is known (Schoof, 2007; Mulder et al., 2018) and consists of two back-to-back saddle-node bifurcations inducing the MISI, resulting in a fast retreat of WAIS as this parameter exceeds the critical value of $\bar{A}_c = 2.87 \cdot 10^{-25}$ Pa^{-3}s^{-1}. In the coupled model, we consider $\bar{A}$ as a linear function of the southern Atlantic Ocean temperature anomaly ΔT_3

$$\bar{A}(T_3) = \frac{\bar{A}^0}{T_3^0}\left[T_3^0 + c_S \Delta T_3\right]. \tag{1}$$

where c_S is a non-dimensional coupling parameter and the parameters $\bar{A}^0$ and T_3^0 indicate values at reference state, translating into into a critical value $\Delta T_{3,c}$ decreasing as c_s increases. Although no straightforward link can be established between T_3 and the regional ocean temperature, let us note that the range $c_S = 0.1 - 0.3$ corresponds to the range $\Delta T_{3,c} = 0.4{-}1.2$, similar to model predictions for the regional ocean warming likely to trigger a WAIS tipping (Garbe et al., 2020; Mas e Braga et al., 2021; Rosier et al., 2021). Finally, ice loss is converted into a meltwater flux F_S, from which we assume only a fraction $f = 0.27$ to enter the southern Atlantic Ocean, considering the rest to be lost in the Pacific Ocean. More details about the WAIS model and the estimation of f are provided in the section S3 of the SI.

3 Results

In this section, we will systematically use the initial state such that the AMOC is in a stable northern-sinking configuration similar to present-day (Lucarini & Stone, 2005), and with ice sheets yielding realistic values for ice volumes and meltwater fluxes (see section S4 of the SI). To investigate the coupled model under global warming, we linearly increase surface temperatures over the GIS and Atlantic Ocean during 100 years, after which temperature is held constant, i.e. for $j \in \{N, 1, 2, 3\}$ (with t in years),

$$\tau_j(t) = \tau_j(0) + \gamma_j \frac{\Delta\tau_2}{100} t. \tag{2}$$

where amplification parameters γ_j are used to represent the phenomena of polar amplification (Hahn et al., 2021; Holland & Landrum, 2021; Cai et al., 2021), here with respect to the equatorial warming $\Delta\tau_2$. Those are estimated from results of Hahn et al. (2021), where many CMIP5 and CMIP6 models were used and compared to assess the (zonally averaged) amplification as a function of latitude when forced by a CO_2 quadrupling, and chosen to be $\gamma_N = 2$, $\gamma_1 = 1.3$, $\gamma_2 = 1.0$ and $\gamma_3 = 1.0$. For those values, the forcing can be expressed in terms of the global warming $\Delta\tau_G \approx 1.1\Delta\tau_2$ alone, obtained by averaging over the Earth's surface.

To determine whether cascading occurs or not, we first focus on the AMOC when no ice sheets are involved or, in other words, when $c_S = \gamma_N = 0$. In this case, applying the forcing (2), we find a critical value $\Delta\tau_{G,c} = 8.1$ °C at which the AMOC destabilizes, thereby tipping to the southern sinking configuration. Next, we couple only the GIS to the AMOC, i.e. setting $c_S = 0$. The critical value $\Delta\tau_{G,c}$, above which the AMOC destabilizes decreases to 5.8 °C. As the GIS reaches its critical warming level already at

$\Delta\tau_N = 1.2°C$ (or $\Delta\tau_G = 0.7°C$), the AMOC is destabilized not only by rising temperatures but also by additional meltwater input into the northern box from the GIS. This situation clearly represents a tipping cascade as both systems tip while only the critical threshold of the GIS has been crossed.

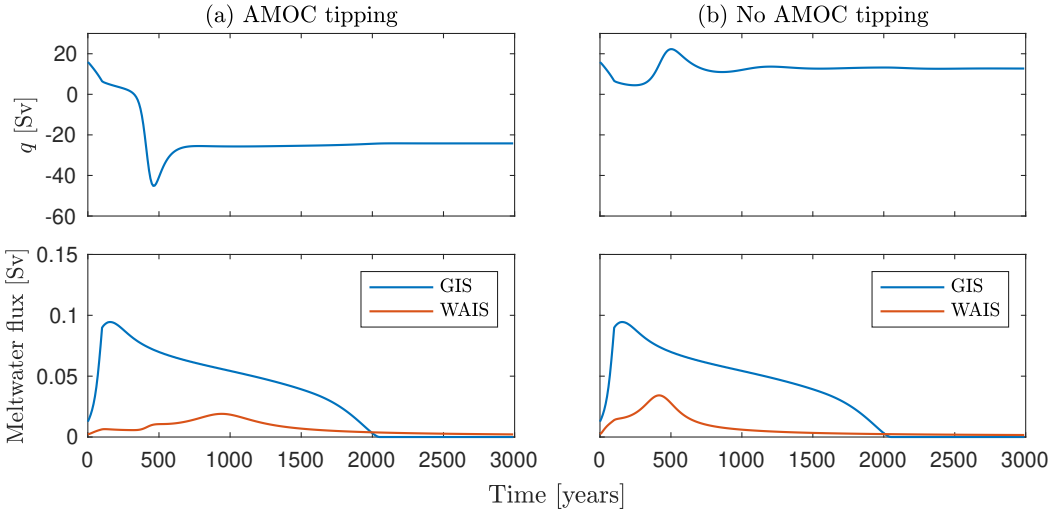

Figure 2. *Transient behavior of the AMOC strength q and the ice sheet meltwater fluxes under a linear climate warming of $\Delta\tau_G = 6\,°C$ lasting 100 yrs, for different couplings: (a) $c_S = 0.2$ and (b) $c_S = 0.8$.*

Finally, choosing non-zero values for c_S, we couple the WAIS to the system. We repeat the global warming experiments with $\Delta\tau_G = 6°C$ for two different WAIS-coupling values, $c_S = 0.2$ and $c_S = 0.8$. For this level of warming, the GIS systematically tips at about year 10, while T_3 is increased by approximately 5 °C, far above the critical value triggering the MISI for both c_S values.

In the case of low coupling ($c_S = 0.2$, Fig. 2.a), the WAIS tips at about year 30, and the resulting meltwater flux is not large enough to compensate for the destabilizing effect of freshwater input in the north. Hence, the AMOC tips at about 400 years, resulting in another drastic rise of T_3. However, the subsequent acceleration of the WAIS collapse happens too late, as the AMOC is then already in a reversed circulation regime. Higher coupling ($c_S = 0.8$, Fig. 2.b) results in a more abrupt WAIS collapse triggered earlier, at about year 10. In this case, the meltwater flux is strong enough to maintain the AMOC in a northern sinking configuration. It is worth noting however that, while the circulation shift has been avoided, the AMOC stregnth is commited to a long term decrease of about 20 percent due to global warming.

The cases in Fig. 2 are shown as the red crosses in Fig. 3a, where the final state of the AMOC is shown in part of the ($\Delta\tau_G$, c_S) parameter plane. In the yellow region, the AMOC is destabilized to the southern sinking state while, in the blue region, it remains in a northern sinking configuration. As expected, the critical value of warming leading to AMOC tipping $\Delta\tau_{G,c}$ (the boundary between the yellow and blue region) increases with increasing c_S, i.e. when the WAIS more strongly reacts to ocean warming. Over the c_S interval $[0, 1]$, meaning for critical values of ocean warming $\Delta T_{3,c}$ going as low as 0.1 °C, $\Delta\tau_{G,c}$ is risen by 0.47 °C. Hence, this creates the possibility of preventing a collapse of the AMOC under the conditions for which the WAIS tips fast enough. Impor-

tantly, this range of increase linearly depends on the fraction f of the WAIS meltwater flux reaching the southern Atlantic Ocean (see Fig. S1 of the SI).

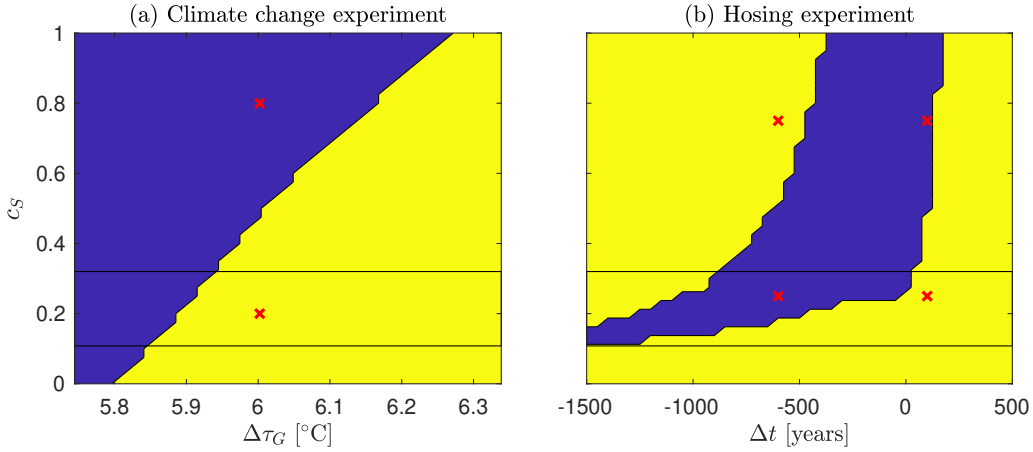

Figure 3. *(a) Final state of the AMOC depending on the climate change $\Delta\tau_G$ and coupling constant c_S. (b) Same for the hosing experiment but depending on the time delay Δt and coupling constant c_S. The yellow area stands for reversed circulation (tipping), while blue area stands for northern sinking circulation (no tipping). The two black rectangles frame the region where the coupling c_S corresponds to the range of critical ocean warming $\Delta T_{3,c} = 0.4 - 1.2\,^\circ C$. Red crosses represent parameter configurations used in (a) Fig. 2 and (b) Fig. S2 of the SI.*

In the global warming experiments so far, the destabilization of the three tipping elements is induced within a short forcing time of 100 yrs. Moreover, at initial state, all tipping elements are in equilibrium while in reality, some of them might already be engaged in a transient, e.g. the GIS or WAIS. To gain more insight into the influence of the different delays and rates of change in the coupled system, we perform additional sensitivity experiments by forcing only the ice sheets, while the AMOC reacts solely to the implied meltwater fluxes, similar to what is seen in so-called hosing experiments (Rahmstorf et al., 2005).

First, we apply a linear increase of the regional surface temperature in Greenland τ_N lasting 100 years, and look for the critical value of $\Delta\tau_N$ leading to a southern sinking state of the AMOC. At the critical value of $\Delta\tau_{N,c} = 22.3$ °C, the AMOC tipping occurs at a GIS melting totally in about 500 years. With this forcing, the GIS meltwater flux reaches 0.33 Sv, which is less than the forcing required to reach the Hopf bifurcation of the Rooth model. Hence, the AMOC collapse cannot be explained by bifurcation tipping. However, as the GIS collapses, the meltwater flux increases fast enough to trigger a rate-induced tipping (Ashwin et al., 2012).

Next, we add the WAIS to assess the stability of the AMOC when interacting with both polar ice sheets. To explore the combined effect of tipping rates and their delay in time, we force both ice sheets independently. At a time t we initiate a forcing of the GIS, linearly increasing τ_N by 23°C in 100 years. By choosing a slightly larger forcing than in the previous experiment, we reduce the potential AMOC stabilizing region occurring as a consequence of the WAIS tipping. After a time delay Δt, we initiate a forcing of the WAIS, applying a linear increase of T_3 by 7°C (affecting the WAIS only), in 100 years. Here, the exact value of T_3 increase is not crucial as the WAIS tipping response will anyway be determined by the coupling parameter c_S.

The final state of the AMOC in the parameter space $(\Delta t, c_S)$ is shown in Fig. 3b. Below $c_S \approx 0.1$ (hence above $\Delta T_{3,c} = 1.3°C$), the AMOC always tips whenever the WAIS forcing is initiated. In this case, no WAIS meltwater flux can stabilize the AMOC against the high GIS meltwater input. However, as the coupling constant c_S increases, a region of stability appears (blue). In this region, the lowest values of c_S require a strongly negative time delay Δt to prevent the AMOC tipping. There, the slower WAIS tipping provides a lower but sufficiently sustained meltwater input, such that the peak of the MISI coincides with the fast GIS tipping. As c_S increases, the stabilizing region rapidly encompasses shorter delays, including positive ones from $c_S \approx 0.3$. Note however that, at strong coupling, a WAIS tipping triggered too soon will result in all the WAIS meltwater content to be released too long before the GIS tipping. Finally, it appears that there is a critical time delay at about $\Delta t = 200$ years, from which no WAIS tipping can causally interfere with the destabilization of the AMOC, due to the strong hysteresis behavior of the Rooth model. Representative cases (red crosses in Fig. 3b) are represented on the Fig. S2 of the SI.

4 Summary and Discussion

In this paper, we present a conceptual model to study the interaction of three tipping elements (WAIS, AMOC and the GIS) of the climate system. Under global warming, coupling the GIS to the AMOC drastically destabilizes the AMOC, making the GIS a potential initiator of global cascading as suggested by Wunderling et al. (2021). On the other hand, coupling the WAIS to the AMOC has a stabilizing effect on the AMOC, especially in the case of a relatively fast and early WAIS tipping.

By considering the stability of the AMOC when affected by meltwater fluxes only, we identified two key components to prevent an AMOC collapse, i.e. interrupting a tipping cascade: the tipping rate of ice masses and the time delay between these tipping phenomena. While a comparatively slow tipping of the WAIS could keep the AMOC stable when triggered hundreds of years before the GIS tipping, it turns out that a faster WAIS tipping is more efficient to avoid an AMOC collapse for shorter delays, which is probably a more realistic scenario when thinking about climate change. In any case, our results rely on the fact that a freshwater input in the southern Atlantic Ocean stabilizes the AMOC, a behavior which is shared by many box model representations of the AMOC (Rooth, 1982; Rahmstorf, 1996; Cimatoribus et al., 2012).

Of course, the model contains many idealizations and hence we argue below why we think these results are robust when more detailed physical processes are included. First, it is known that the stability of the AMOC in the Rooth model is very sensitive to the inter-hemispheric temperature forcing asymmetry, here implied by the amplification coefficients used to define climate change (Lucarini & Stone, 2005). While other choices of these parameters would affect the magnitude of the GIS and WAIS influence on the AMOC stability, we expect our results remain robust as long as the warming remains destabilizing. A more accurate assessment of those amplification coefficients spanning the Atlantic Ocean alone would be an improvement to the quantitative results of our study.

Second, the description of the influence of the oceanic temperature on the WAIS has been strongly idealized. However, we can expect our qualitative results to hold as long as this interaction remains destabilizing. To better base it on physical grounds, one would have to consider sub-shelf melting and calving processes, interacting with the ice shelf stability through buttressing (Haseloff & Sergienko, 2018, 2022) and lateral drag (Schoof et al., 2017). Also, a better assessment of the fraction f of the WAIS freshwater flux reaching the southern Atlantic Ocean would be a direct improvement, which involves resolving the dynamics associated to the Antarctic Circumpolar Current, which is beyond the scope of this study. Nonetheless, the apparent linear behavior of the crit-

ical warming with respect to f supports our results, as the stabilizing effect remains substantial when f varies around our estimation.

Third, some feedbacks have been omitted. The stabilizing effect of an AMOC tipping on the GIS, as well as the mutually destabilizing effect of sea level rise (Gomez et al., 2010) on both ice sheets have been neglected. While the former is not expected to interfere with the AMOC stability due to the strong hysteresis behavior of the Rooth model, the latter would most probably strengthen the AMOC stabilization, as the sea level interaction is far more destabilizing for the WAIS (Wunderling et al., 2021).

In conclusion, the stability of the climate system, and in particular of the AMOC, is drastically changed when considering interactions between the tipping elements in agreement with the more abstract results of Wunderling et al. (2021). We emphasized here the consequences of a potentially stabilizing effect of a WAIS tipping on the AMOC in the presence of a tipping GIS, which could have important consequences on the other tipping elements. For example, the Amazon rainforest is potentially strongly influenced by the AMOC (Parsons et al., 2014). Hence, while the collapse of the WAIS will always be a dramatic event, it might prevent a larger-scale cascading tipping event to happen. This stresses the importance of getting a better understanding of the interaction between the WAIS and the AMOC and to include the effects of interacting tipping elements in future climate change projections.

5 Open Research

All MATLAB codes are publicly available (Sinet, 2022), at the address https://doi.org/10.5281/zenodo.6800143

Acknowledgments

This project has received funding from the European Union's Horizon 2020 research and innovation programme under the Marie Skłodowska-Curie Grant Agreement No. 956170 (CriticalEarth). We thank V. Lucarini for helpful discussions.

References

Ashwin, P., Wieczorek, S., Vitolo, R., & Cox, P. (2012). Tipping points in open systems: bifurcation, noise-induced and rate-dependent examples in the climate system. *Philosophical Transactions of the Royal Society A: Mathematical, Physical and Engineering Sciences*, *370*(1962), 1166-1184. doi: 10.1098/rsta.2011.0306

Bakker, P., Schmittner, A., Lenaerts, J. T. M., Abe-Ouchi, A., Bi, D., van den Broeke, M. R., ... Yin, J. (2016). Fate of the Atlantic Meridional Overturning Circulation: strong decline under continued warming and greenland melting. *Geophysical Research Letters*, *43*(23), 12,252-12,260. doi: https://doi.org/10.1002/2016GL070457

Benn, D. I., Hulton, N. R., & Mottram, R. H. (2007). 'calving laws', 'sliding laws' and the stability of tidewater glaciers. *Annals of Glaciology*, *46*, 123–130. doi: 10.3189/172756407782871161

Boers, N. (2021). Observation-based early-warning signals for a collapse of the Atlantic Meridional Overturning Circulation. *Nature Climate Change*, *11*(8), 680-688. doi: 10.1038/s41558-021-01097-4

Boers, N., & Rypdal, M. (2021). Critical slowing down suggests that the Western Greenland Ice Sheet is close to a tipping point. *Proceedings of the National Academy of Sciences*, *118*(21), e2024192118. doi: 10.1073/pnas.2024192118

Bueler, E., Lingle, C. S., Kallen-Brown, J. A., Covey, D. N., & Bowman, L. N. (2005). Exact solutions and verification of numerical models for isother-

mal ice sheets. *Journal of Glaciology*, *51*(173), 291–306. doi: 10.3189/172756505781829449

Caesar, L., McCarthy, G., Thornalley, D., Cahill, N., & Rahmstorf, S. (2021). Current Atlantic Meridional Overturning Circulation weakest in last millennium. *Nature Geoscience*, *14*, 1-3. doi: 10.1038/s41561-021-00699-z

Caesar, L., Rahmstorf, S., Robinson, A., Feulner, G., & Saba, V. (2018). Observed fingerprint of a weakening Atlantic Ocean overturning circulation. *Nature*, *556*, 191–196. doi: 10.1038/s41586-018-0006-5

Cai, S., Hsu, P.-C., & Liu, F. (2021). Changes in polar amplification in response to increasing warming in CMIP6. *Atmospheric and Oceanic Science Letters*, *14*(3), 100043. doi: https://doi.org/10.1016/j.aosl.2021.100043

Cimatoribus, A. A., Drijfhout, S. S., & Dijkstra, H. A. (2012). Meridional overturning circulation: stability and ocean feedbacks in a box model. *Climate Dynamics*, *42*(1–2), 311–328. doi: 10.1007/s00382-012-1576-9

Dekker, M. M., von der Heydt, A. S., & Dijkstra, H. A. (2018). Cascading transitions in the climate system. *Earth System Dynamics*, *9*(4), 1243–1260. doi: 10.5194/esd-9-1243-2018

Enderlin, E., Howat, I., Jeong, S., Noh, M.-J., van angelen, J., & Van den Broeke, M. (2014). An improved mass budget for the Greenland Ice Sheet. *Geophysical Research Letters*, *41*(3), 866-872. doi: 10.1002/2013GL059010

Favier, L., Durand, G., Cornford, S., Gudmundsson, G., Gagliardini, O., Gillet-Chaulet, F., ... Brocq, A. (2014). Retreat of Pine Island Glacier controlled by marine ice-sheet instability. *Nature Climate Change*, *4*(2), 117-121. doi: 10.1038/nclimate2094

Favier, L., Jourdain, N. C., Jenkins, A., Merino, N., Durand, G., Gagliardini, O., ... Mathiot, P. (2019). Assessment of sub-shelf melting parameterisations using the ocean–ice-sheet coupled model NEMO(v3.6)–Elmer/Ice(v8.3). *Geoscientific Model Development*, *12*(6), 2255–2283. doi: 10.5194/gmd-12-2255-2019

Feldmann, J., & Levermann, A. (2015). Collapse of the West Antarctic Ice Sheet after local destabilization of the Amundsen Basin. *Proceedings of the National Academy of Sciences*, *112*, 14191-14196. doi: 10.1073/pnas.1512482112/-/DCSupplemental

Garbe, J., Albrecht, T., Levermann, A., Donges, J., & Winkelmann, R. (2020). The hysteresis of the Antarctic Ice Sheet. *Nature*, *585*, 538-544. doi: 10.1038/s41586-020-2727-5

Glorot, X., Bordes, A., & Bengio, Y. (2011). Deep sparse rectifier neural networks. In *Proceedings of the fourteenth international conference on artificial intelligence and statistics* (Vol. 15, pp. 315–323). Fort Lauderdale, FL, USA: Proceedings of Machine Learning Research.

Goelzer, H., Huybrechts, P., Fürst, J., Nick, F., Andersen, M., Edwards, T., ... Shannon, S. (2013). Sensitivity of Greenland Ice Sheet projections to model formulations. *Journal of Glaciology*, *59*(216), 733–749. doi: 10.3189/2013JoG12J182

Gomez, N., Mitrovica, J. X., Huybers, P., & Clark, P. U. (2010). Sea level as a stabilizing factor for marine-ice-sheet grounding lines. *Nature Geoscience*, *3*(12), 850–853. doi: 10.1038/ngeo1012

Greve, R., & Blatter, H. (2009). *Dynamics of ice sheets and glaciers.* Berlin, Germany: Springer.

Hahn, L. C., Armour, K. C., Zelinka, M. D., Bitz, C. M., & Donohoe, A. (2021). Contributions to polar amplification in CMIP5 and CMIP6 models. *Frontiers in Earth Science*, *9*, 710036. doi: 10.3389/feart.2021.710036

Haseloff, M., & Sergienko, O. V. (2018). The effect of buttressing on grounding line dynamics. *Journal of Glaciology*, *64*(245), 417–431. doi: 10.1017/jog.2018.30

Haseloff, M., & Sergienko, O. V. (2022). Effects of calving and submarine melting on steady states and stability of buttressed marine ice sheets. *Journal of Glaciol-*

ogy, 1–18. doi: 10.1017/jog.2022.29

Holland, M. M., & Landrum, L. (2021). The emergence and transient nature of Arctic amplification in coupled climate models. *Frontiers in Earth Science*, *9*, 719024. doi: 10.3389/feart.2021.719024

Irvalı, N., Galaasen, E. V., Ninnemann, U. S., Rosenthal, Y., Born, A., & Kleiven, H. K. F. (2020). A low climate threshold for South Greenland Ice Sheet demise during the late Pleistocene. *Proceedings of the National Academy of Sciences*, *117*(1), 190–195. doi: 10.1073/pnas.1911902116

Jackson, L. C., & Wood, R. A. (2018). Hysteresis and resilience of the AMOC in an eddy-permitting GCM. *Geophysical Research Letters*, *45*(16), 8547-8556. doi: https://doi.org/10.1029/2018GL078104

Joughin, I., Smith, B. E., & Medley, B. (2014). Marine ice sheet collapse potentially under way for the Thwaites Glacier Basin, West Antarctica. *Science*, *344*(6185), 735-738. doi: 10.1126/science.1249055

Klose, A. K., Wunderling, N., Winkelmann, R., & Donges, J. F. (2021). What do we mean, 'tipping cascade'? *Environmental Research Letters*, *16*(12), 125011. doi: 10.1088/1748-9326/ac3955

Kriegler, E., Hall, J. W., Held, H., Dawson, R., & Schellnhuber, H. J. (2009). Imprecise probability assessment of tipping points in the climate system. *Proceedings of the National Academy of Sciences*, *106*(13), 5041-5046. doi: 10.1073/pnas.0809117106

Lenaerts, J., Le Bars, D., van Kampenhout, L., Vizcaíno, M., Enderlin, E., & Van den Broeke, M. (2015). Representing Greenland Ice Sheet freshwater fluxes in climate models. *Geophysical Research Letters*, *42*, 6373-6381. doi: 10.1002/2015GL064738

Lenton, T. M., Held, H., Kriegler, E., Hall, J. W., Lucht, W., Rahmstorf, S., & Schellnhuber, H. J. (2008). Tipping elements in the earth's climate system. *Proceedings of the National Academy of Sciences*, *105*(6), 1786–1793. doi: 10.1073/pnas.0705414105

Levermann, A., & Winkelmann, R. (2016). A simple equation for the melt elevation feedback of ice sheets. *The Cryosphere*, *10*(4), 1799–1807. doi: 10.5194/tc-10-1799-2016

Lucarini, V., & Stone, P. H. (2005). Thermohaline circulation stability: a box model study. Part I: uncoupled model. *Journal of Climate*, *18*(4), 501 - 513. doi: 10.1175/JCLI-3278.1

Mas e Braga, M., Bernales, J., Prange, M., Stroeven, A. P., & Rogozhina, I. (2021). Sensitivity of the antarctic ice sheets to the warming of marine isotope substage 11c. *The Cryosphere*, *15*(1), 459–478. Retrieved from `https://tc.copernicus.org/articles/15/459/2021/` doi: 10.5194/tc-15-459-2021

McCarthy, G. D., Smeed, D. A., Johns, W. E., Frajka-Williams, E., Moat, B. I., Rayner, D., ... Bryden, H. L. (2015). Measuring the Atlantic Meridional Overturning Circulation at 26°N. *Progress in Oceanography*, *103*, 91–111.

Morlighem, M., Rignot, E., Binder, T., Blankenship, D., Drews, R., Eagles, G., ... Young, D. (2020). Deep glacial troughs and stabilizing ridges unveiled beneath the margins of the Antarctic ice sheet. *Nature Geoscience*, *13*, 1-6. doi: 10.1038/s41561-019-0510-8

Morlighem, M., Williams, C. N., Rignot, E., An, L., Arndt, J. E., Bamber, J. L., ... Zinglersen, K. B. (2017). BedMachine v3: Complete bed topography and ocean bathymetry mapping of Greenland from multibeam echo sounding combined with mass conservation. *Geophysical Research Letters*, *44*(21), 11,051-11,061. doi: https://doi.org/10.1002/2017GL074954

Mulder, T. E., Baars, S., Wubs, F. W., & Dijkstra, H. A. (2018). Stochastic marine ice sheet variability. *Journal of Fluid Mechanics*, *843*, 748–777. doi: 10.1017/jfm.2018.148

Parsons, L. A., Yin, J., Overpeck, J. T., Stouffer, R. J., & Malyshev, S. (2014).

Influence of the atlantic meridional overturning circulation on the monsoon rainfall and carbon balance of the american tropics. *Geophysical Research Letters*, *41*(1), 146-151. doi: https://doi.org/10.1002/2013GL058454

Rahmstorf, S. (1996). On the freshwater forcing and transport of the atlantic thermohaline circulation. *Climate Dynamics*, *12*, 799-811.

Rahmstorf, S., Crucifix, M., Ganopolski, A., Goosse, H., Kamenkovich, I., Knutti, R., ... Weaver, A. J. (2005). Thermohaline circulation hysteresis: A model intercomparison. *Geophysical Research Letters*, *32*(23), L23605. doi: https://doi.org/10.1029/2005GL023655

Ridley, J., Gregory, J., Huybrechts, P., & Lowe, J. (2009). Thresholds for irreversible decline of the Greenland ice Sheet. *Climate Dynamics*, *35*, 1049-1057. doi: 10.1007/s00382-009-0646-0

Rignot, E., Mouginot, J., Morlighem, M., Seroussi, H., & Scheuchl, B. (2014). Widespread, rapid grounding line retreat of Pine Island, Thwaites, Smith, and Kohler glaciers, West Antarctica, from 1992 to 2011. *Geophysical Research Letters*, *41*(10), 3502-3509.

Rignot, E., Mouginot, J., Scheuchl, B., van den Broeke, M. R., van Wessem, M., & Morlighem, M. (2019). Four decades of Antarctic Ice Sheet mass balance from 1979–2017. *Proceedings of the National Academy of Sciences of the United States of America*, *116*, 1095 - 1103.

Robinson, A., Calov, R., & Ganopolski, A. (2012). Multistability and critical thresholds of the Greenland Ice Sheet. *Nature Climate Change*, *2*, 429-432. doi: 10.1038/nclimate1449

Rooth, C. (1982). Hydrology and ocean circulation. *Progress in Oceanography*, *11*(2), 131-149. doi: https://doi.org/10.1016/0079-6611(82)90006-4

Rosier, S. H. R., Reese, R., Donges, J. F., De Rydt, J., Gudmundsson, G. H., & Winkelmann, R. (2021). The tipping points and early warning indicators for pine island glacier, west antarctica. *The Cryosphere*, *15*(3), 1501–1516. Retrieved from `https://tc.copernicus.org/articles/15/1501/2021/` doi: 10.5194/tc-15-1501-2021

Schellnhuber, H., Rahmstorf, S., & Winkelmann, R. (2016). Why the right climate target was agreed in Paris. *Nature Climate Change*, *6*, 649-653. doi: 10.1038/nclimate3013

Schoof, C. (2007). Ice sheet grounding line dynamics: Steady states, stability, and hysteresis. *Journal of Geophysical Research*, *112*, F03S28. doi: 10.1029/2006JF000664

Schoof, C., Davis, A. D., & Popa, T. V. (2017). Boundary layer models for calving marine outlet glaciers. *The Cryosphere*, *11*(5), 2283–2303. doi: 10.5194/tc-11-2283-2017

Schoof, C., & Hewitt, I. (2013). Ice-sheet dynamics. *Annual Review of Fluid Mechanics*, *45*(1), 217-239. doi: 10.1146/annurev-fluid-011212-140632

Scott, J. R., Marotzke, J., & Stone, P. H. (1999). Interhemispheric thermohaline circulation in a coupled box model. *Journal of Physical Oceanography*, *29*(3), 351 - 365. doi: 10.1175/1520-0485(1999)029⟨0351:ITCIAC⟩2.0.CO;2

Shepherd, A., Wingham, D., & Rignot, E. (2004). Warm ocean is eroding West Antarctic Ice Sheet. *Geophysical Research Letters*, *31*(23), L23402. doi: https://doi.org/10.1029/2004GL021106

Sinet, S. (2022). *AMOC Stabilisation under the Interaction with Tipping Polar Ice Sheets [Software].* Zenodo. Retrieved from `https://doi.org/10.5281/zenodo.6800143` doi: 10.5281/zenodo.6800143

Swingedouw, D., Fichefet, T., Goosse, H., & Loutre, M.-F. (2008). Impact of transient freshwater releases in the Southern Ocean on the amoc and climate. *Climate Dynamics*, *33*, 365-381. doi: 10.1007/s00382-008-0496-1

The IMBIE Team. (2018). Mass balance of the Antarctic Ice Sheet from 1992 to 2017. *Nature*, *558*, 219-222. doi: 10.1038/s41586-018-0179-y

The IMBIE Team. (2020). Mass balance of the Greenland Ice Sheet from 1992 to 2018. *Nature*, *579*, 233–239. doi: 10.1038/s41586-019-1855-2

Titz, S., Kuhlbrodt, T., Rahmstorf, S., & Feudel, U. (2002). On freshwater-dependent bifurcations in box models of the interhemispheric thermohaline circulation. *Tellus A: Dynamic Meteorology and Oceanography*, *54*(1), 89-98. doi: 10.3402/tellusa.v54i1.12126

Van Den Berg, J., Van De Wal, R., & Oerlemans, J. (2006). Effects of spatial discretization in ice-sheet modelling using the shallow-ice approximation. *Journal of Glaciology*, *52*(176), 89–98. doi: 10.3189/172756506781828935

Weertman, J. (1974). Stability of the junction of an ice sheet and an ice shelf. *Journal of Glaciology*, *13*(67), 3–11. doi: 10.3189/S0022143000023327

Wunderling, N., Donges, J. F., Kurths, J., & Winkelmann, R. (2021). Interacting tipping elements increase risk of climate domino effects under global warming. *Earth System Dynamics*, *12*(2), 601–619. doi: 10.5194/esd-12-601-2021

Supporting Information for "AMOC Stabilization under the Interaction with Tipping Polar Ice Sheets"

S. Sinet[1,2], A. S. von Der Heydt[1,2], and H. A. Dijkstra[1,2]

[1]Department of Physics, Institute for Marine and Atmospheric Research Utrecht, Utrecht University, Utrecht, The Netherlands

[2]Center for Complex Systems Studies, Department of Physics, Utrecht University, Utrecht, The Netherlands

Contents of this file

Introduction

In this document, we provide a more detailed description of the Greenland Ice Sheet (GIS), Atlantic Meridional Overturning Circulation (AMOC) and West Antarctica Ice Sheet (WAIS) models through texts S1 to S3, and describe the construction of the initial state in the text S4. Finally, we describe our numerical resolution in section S5.

S1. The GIS model

We consider an isothermal ice sheet lying on a fixed bedrock (Greve & Blatter, 2009). The evolution of the ice thickness h is given by the contribution of the transport inside the ice dome involving the ice flux F, along with the Surface Mass Balance (SMB) a (positive or negative in case of respectively freezing or melting), condensed in the continuity equation

$$\frac{\partial h}{\partial t} = -\nabla \cdot F + a. \tag{1}$$

In the case of an isothermal ice sheet, the problem is simplified by using the Shallow Ice Approximation (SIA) giving an expression for the flux. To simplify the problem further, we consider a radially symmetric ice cap resting on a flat circular bed of radius R at sea level. Also, the SMB will be expressed as a function of the ice elevation alone such that, in polar coordinates, the system of equations is

$$\frac{\partial h}{\partial t} = -\frac{1}{r}\frac{\partial}{\partial r}(rF) + a(h) \tag{2}$$

$$F = -A_0 \frac{\partial h}{\partial r}\left|\frac{\partial h}{\partial r}\right|^{n-1} h^{n+2}, \tag{3}$$

to which we add the no-ice condition $h = 0$ for $r \geq L(t)$, where we denote by $L(t)$ the radial position of the ice margin, such that $L(t) \leq R$ at all time. Also,

$$A_0 = \frac{2A(\rho_i g)^n}{n+2}, \tag{4}$$

where A is the ice viscosity parameter, ρ_i the ice density, g the gravitational acceleration and n the exponent used in the Glenn's flow law. This system describes a free boundary problem (Schoof & Hewitt, 2013) and, in this case of purely height-dependant SMB, the domain at steady state will necessarily be totally ice-covered or ice-free. Solving this

equation numerically is subtle, and our approach is presented in the text S5.1. Following (Greve & Blatter, 2009), we represent the height-SMB feedback by expressing a in a simple form, involving only three parameters

$$a(h) = \min\left[P, m\left(h - h_{el}\right)\right], \tag{5}$$

namely the melting gradient m, the precipitation rate P and the equilibrium line altitude h_{el}. The latter two are made temperature dependant by assuming that their present-day (inter glacial) and glacial climate values are linearly related with respect to the temperature anomaly in the northern hemisphere $\Delta\tau_N$. It means

$$P(\Delta\tau_{\mathrm{N}}) = P_{IG} + \frac{P_G - P_{IG}}{\Delta\tau_{N,G}}\Delta\tau_{\mathrm{N}},$$
$$h_{el}(\Delta\tau_{\mathrm{N}}) = h_{el,IG} + \frac{h_{el,\mathrm{G}} - h_{el,IG}}{\Delta\tau_{N,G}}\Delta\tau_{\mathrm{N}},$$

where indexes G and IG stand for respectively the glacial and inter glacial climates. All parameter values are presented in table S1.

To compute the meltwater flux F_N, we express mass conservation by integrating the continuity equation 2 over the whole domain. Performing the integration and using the Leibniz integral rule for the l.h.s. we get, considering that $h(L(t)) = 0$ by definition,

$$\frac{\partial V}{\partial t} = -2\pi L(t)F(L(t)) + 2\pi\int_0^{L(t)} a(h)r dr. \tag{6}$$

The SMB can be separated into a precipitation component P and a melting component M. Consistently with equation 5, P is constant over the domain such that we can write

$$\frac{\partial V}{\partial t} = \pi L^2(t)P - 2\pi L(t)F(L(t)) + 2\pi\int_0^{L(t)} M(h)r dr. \tag{7}$$

In the r.h.s, the outflux is represented by calving (second term) and melting (third term). Hence, we define the meltwater flux positively as

$$F_N = \frac{\rho_i}{\rho_w}\left(\pi L^2(t)P - \frac{\partial V}{\partial t}\right), \tag{8}$$

where the prefactor ρ_i/ρ_w stands for the conversion of the ice volume into a water volume.

S2. The AMOC model

We use the model of Rooth (Rooth, 1982) as presented in (Lucarini & Stone, 2005), where the AMOC is depicted by 3 boxes yielding a thermohaline circulation driven by the pole-to-pole density difference. Respectively, the first box represents the northern Atlantic Ocean above 30°N, the second box represents the tropical region between 30°N and 30°S, and the third box represents the southern Atlantic Ocean under 30°S. Hence, to some approximation, the equatorial box is two times the volume of each polar boxes, defining the box volume ratio $V = V_2/V_1 = V_2/V_3 = 2$. From the temperature T_j and salinity S_j of one box, the density ρ_j for $j = \{1, 2, 3\}$ is approximated by

$$\rho_j(T_j, S_j) \approx \rho_w(1 - \alpha T_j + \beta S_j), \tag{9}$$

where ρ_w is the reference water density, α is the thermal expansion coefficient and β the haline expansion coefficient. The AMOC strength q is then directly computed using the normalised pole-to-pole density difference

$$q = \frac{k}{\rho_w}(\rho_1 - \rho_3) \tag{10}$$

$$= k\left[\alpha\left(T_3 - T_1\right) + \beta\left(S_1 - S_3\right)\right], \tag{11}$$

with k the hydraulic constant, used for fitting q to a reasonable value. Considering a circulation with northern sinking ($q > 0$), the dynamical equations are given by the

variation of temperatures and salinities

$$\frac{\partial T_1}{\partial t} = q\,(T_2 - T_1) + \lambda(\tau_1 - T_1), \tag{12}$$
$$\frac{\partial T_2}{\partial t} = \frac{q}{V}\,(T_3 - T_2) + \lambda(\tau_2 - T_2), \tag{13}$$
$$\frac{\partial T_3}{\partial t} = q\,(T_1 - T_3) + \lambda(\tau_3 - T_3), \tag{14}$$
$$\frac{\partial S_1}{\partial t} = q\,(S_2 - S_1) - (\bar{F}_1 + \bar{F}_N), \tag{15}$$
$$\frac{\partial S_2}{\partial t} = \frac{q}{V}\,(S_3 - S_2) + \frac{(\bar{F}_1 + \bar{F}_N + \bar{F}_3 + \bar{F}_S)}{V}, \tag{16}$$
$$\frac{\partial S_3}{\partial t} = q\,(S_1 - S_3) - (\bar{F}_3 + \bar{F}_S). \tag{17}$$

All the parameters involved are presented in table S1. Both temperatures and salinities are transported via an advection term implying the AMOC strength q. The temperature of each box is relaxed to a target temperatures τ_i, at a timescale given by the relaxation constant λ (corresponding to about 25 yr). Salinities are forced by freshwater fluxes including precipitation $F_{1,3}$ and meltwater fluxes $F_{N,S}$ in the poles, compensated by evaporation in the tropics. In the equations, those are expressed by virtual salinity fluxes $\bar{F}_i$ through scaling, i.e. for $i \in \{1, N, 3, S\}$,

$$\bar{F}_i = \frac{S_0 \rho_w}{M} F_i, \tag{18}$$

where M is the mass of polar boxes and S_0 the average salinity. Note that the evaporation term in equation 16 imposes average salinity conservation. Finally, this model applied to a southern sinking configuration implies a permutation of temperatures and salinites in the r.h.s. of each equation (Scott et al., 1999). The system is not differentiable at this transition - we show in the text S5.2 how to handle it in our numerical resolution.

S3. The WAIS model

The WAIS, here considered as one single Marine Ice Sheet (MIS), is represented using a depth integrated Shallow Shelf Approximation (SSA) as in (Schoof, 2007). In the case of a rapidly sliding, two-dimensional and symmetrical MIS, the dynamical equations are given by

$$\frac{\partial h}{\partial t} + \frac{\partial (uh)}{\partial x} = a, \tag{19}$$

$$\frac{\partial}{\partial x}\left[2\bar{A}^{-1/n} h \left|\frac{\partial u}{\partial x}\right|^{(1/n)-1} \frac{\partial u}{\partial x}\right] - C|u|^{(m-1)}u - \rho_i g h \frac{\partial (h-b)}{\partial x} = 0. \tag{20}$$

Here, b is the depth of the bedrock (positive when under sea level), u is the depth integrated flow inside the bulk, $\bar{A}$ is the depth integrated viscosity parameter, while C and m define the sliding law. Note that we consider the accumulation a constant in time and over the whole domain. The ice shelve is included as a border condition at the grounding line, i.e. at $x = x_g$,

$$2\bar{A}^{-1/n} \left|\frac{\partial u}{\partial x}\right|^{(1/n)-1} \frac{\partial u}{\partial x} = \frac{1}{2}\left(1 - \frac{\rho_i}{\rho_w}\right)\rho_i g h, \tag{21}$$

to which we add the flotation requirement

$$\rho_i h = \rho_w b. \tag{22}$$

Finally, at $x = 0$, we add the symmetry requirement

$$\frac{\partial (h-b)}{\partial x} = 0. \tag{23}$$

All the parameters involved are defined in table S1. It is important to note that, in what follows, we extend this model to one supplementary horizontal dimension of length y_0 with respect to which the MIS yields translational symmetry.

To compute the hosing flux F_S, we express mass conservation by integrating the continuity equation 19 over the whole domain. Performing the integration and using the Leibniz integral rule for the l.h.s. we get

$$\frac{\partial V}{\partial t} - 2y_0 h(x_g(t)) \frac{\partial x_g(t)}{\partial t} = -2y_0 h(x_g(t)) u(x_g(t)) + 2y_0 \int_0^{x_g(t)} a dx. \tag{24}$$

Here, we consider no surface melting, such that the SMB only contains a constant and homogeneous precipitation rate P. Hence we write

$$\frac{\partial V}{\partial t} = 2y_0 x_g(t) P - 2y_0 h(x_g(t)) \left(u(x_g(t)) - \frac{\partial x_g(t)}{\partial t} \right). \tag{25}$$

The only contribution to outflux is the ice flux through the moving grounding line, analogous to a calving process (Benn et al., 2007). Hence, assuming the ice outflux to instantaneously transform into meltwater, we get the meltwater outflux

$$F_S = 2 \frac{\rho_i}{\rho_w} y_0 h(x_g(t)) \left(u(x_g(t)) - \frac{\partial x_g(t)}{\partial t} \right) f, \tag{26}$$

where the prefactor ρ_i / ρ_w stands for the conversion of the ice volume into a water volume. Also, to consider loss of freshwater into the Pacific Ocean, we add a parameter f fixing the fraction of the total meltwater outflux entering the South Atlantic Ocean. To estimate f, we consider the definition of the WAIS drainage basins of Rignot et al. (2019) used in the Ice sheet Mass Balance Inter-comparison Exercise (IMBIE), and assume only the basins draining into the Ronne ice shelf to contribute to the hosing of the southern Atlantic Ocean. Hence, we approximate f by computing the mass ratio between the Ronne draining basin and the entire WAIS, using present-day values (Morlighem et al., 2020).

S4. Construction of the initial state

At initial state, we want the AMOC to be in a northern sinking configuration similar to present-day. To fix it, we set the total freshwater flux in the polar boxes to the values used in (Lucarini & Stone, 2005). In term of virtual salinity fluxes, we have at initial state (denoted by the exponent 0)

$$\bar{F}_1^0 + \bar{F}_N^0 = 13.50 \cdot 10^{-11} \text{ psu s}^{-1}, \tag{27}$$

$$\bar{F}_3^0 + \bar{F}_S^0 = 9.00 \cdot 10^{-11} \text{ psu s}^{-1}, \tag{28}$$

where $\bar{F}_{S,N}^0$ are given once the initial state of ice caps is fixed. On one hand, the only free parameter to tune for the GIS is the radius of the bedrock R. On the other hand, the WAIS model still contains two free parameters, namely $\bar{A}^0$ and y_0, the first being the depth integrated viscosity parameter at initial state. Those are tuned to fit both ice sheet volumes to present-day values (Morlighem et al., 2017, 2020). Those parameters and relevant quantities are summarised in table S2.

We note that the (total) outflux at initial state is slightly overestimated for both ice sheets when compared to present-day estimations (The IMBIE Team, 2018, 2020), due the the limited degrees of freedom. We prioritized the fit to the volume estimations from the literature as this is the quantity that will ultimately dictate the stabilizing and destabilizing effects. Indeed, meltwater fluxes at initial state are absorbed by the values of $\bar{F}_{1,3}^0$ via equation 27 and 28. Finally, we note that the AMOC strength of the hence constructed initial state is in agreement with the values from the RAPID-AMOC programme (McCarthy et al., 2015).

S5. Numerical resolution

The full model is solved with implicit time stepping, using a monolithic approach. The state vector X is given at any time by

$$X(t) = \begin{bmatrix} x_{\mathrm{WAIS}}(t) \\ x_{\mathrm{AMOC}}(t) \\ x_{\mathrm{GIS}}(t) \end{bmatrix}, \tag{29}$$

such that the whole system can be expressed as

$$B\dot{X}(t) = F(X(t), \mu), \tag{30}$$

with μ some (possibly time dependant) parameters, and B a linear operator. From there, we perform the time integration using a θ-method

$$B\frac{X\left(t_{k+1}\right) - X\left(t_k\right)}{\Delta t} = (1-\theta)F\left(X\left(t_k\right), \mu\right) + \theta F\left(X\left(t_{k+1}\right), \mu\right), \quad \theta \in [0,1]., \tag{31}$$

choosing $\theta = 0.7$. As this equation is generally highly non-linear, solving it requires using a root finding algorithm. We use a Newton iteration, involving the Jacobian of the full system

$$J_{ij}(X) = \frac{\partial F_i(X)}{\partial X_j}, \tag{32}$$

which has the following structure

$$J = \begin{pmatrix} J_{\mathrm{WAIS}} & J_{\mathrm{AMOC}\to\mathrm{WAIS}} & 0 \\ J_{\mathrm{WAIS}\to\mathrm{AMOC}} & J_{\mathrm{AMOC}} & J_{\mathrm{GIS}\to\mathrm{AMOC}} \\ 0 & 0 & J_{\mathrm{GIS}} \end{pmatrix}, \tag{33}$$

Where $J_{\mathrm{WAIS}\to\mathrm{AMOC}}$ and $J_{\mathrm{GIS}\to\mathrm{AMOC}}$ contain the coupling via meltwater fluxes from the ice sheets to the AMOC, while $J_{\mathrm{AMOC}\to\mathrm{WAIS}}$ contains the coupling from the southern Atlantic Ocean temperature to the WAIS via the depth integrated ice viscosity parameter $\bar{A}$. This sparse structure allows to divide the resolution of the Jacobian when performing Newton iterations.

S5.1. The GIS model

Given the radial symmetry, the domain is a straight line of constant length R. We use a staggered grid made of $N = 750$ main points numbered $i = 1, \cdots, N$, and a secondary grid falling in between the main grid points, numbered by half integers $i \pm \frac{1}{2}$. The discretization has been chosen such that the axis of symmetry of the ice cap corresponds to the point $1 - \frac{1}{2}$ while the margin falls at $N + 1$.

The effective diffusivity D is defined on the secondary grid for $i = 1, \cdots, N$ by

$$D_{i+\frac{1}{2}} = \frac{A_0}{2}(r_i + r_{i+1}) \left(\frac{h_i + h_{i+1}}{2} \right)^5 \left(\frac{h_{i+1} - h_i}{\Delta r} \right)^2, \tag{34}$$

so that the flux is given by

$$F_{i+\frac{1}{2}} = -\frac{1}{\Delta r} D_{i+\frac{1}{2}} (h_{i+1} - h_i). \tag{35}$$

While the diffusivity term is not defined at $i = 1 - \frac{1}{2}$, the symmetry of the problem directly gives us the border condition for the flux at the axis of symmetry, $F_{1-\frac{1}{2}} = 0$. The dynamical equation then relates the ice elevation at time n and $n + 1$ in a fully implicit scheme

$$\frac{h_i^{n+1} - h_i^n}{\Delta t} = -\frac{1}{r_i^{n+1} \Delta r} \left(F_{i+\frac{1}{2}}^{n+1} - F_{i-\frac{1}{2}}^{n+1} \right) + a_i^{n+1}. \tag{36}$$

As the implicitness requires differentiability, we truncate the SMB a by smoothening the min function using the primitive of the logistic function, also known as the softplus function, widely used in neural networks, see for example (Glorot et al., 2011). In our case, it takes the form

$$a(h) = m \left[h - \frac{P}{m} - h_{el} - \frac{1}{k} \log \left(e^{k\left(h - \frac{P}{m} - h_{el}\right)} + 1 \right) \right] + P, \tag{37}$$

where it is understood that $P = P(\Delta\tau_N)$ and $h_{el} = h_{el}(\Delta\tau_N)$. k is a convergence parameter which we set to 300.

Note that, during the resolution, all the points of the domain are treated equally, meaning that the ice thickness naturally gets negative on the border and where the is no more ice. Hence, at each time step, all negative thicknesses are set to 0. While this yields significant errors in the position and thickness gradient at the margin, it has been shown to have only little effect on the global behaviour of the ice sheet in the isothermal case, as long as the resolution is high enough (Bueler et al., 2005; Van Den Berg et al., 2006).

In the coupled model, we also need to express margin position $L(t)$ and volume of the ice cap V to compute the meltwater outflux. As each time step potentially involves negative ice thicknesses, those quantities involve integrals on the ice covered domain only, hence on the domain $[0\ L(t)]$. However, they can be defined by integrating on the whole domain $[0\ R]$ using a theta function. Respectively,

$$L(t) = \int_0^{L(t)} \mathrm{d}r \tag{38}$$

$$= \int_0^R \Theta\left[h(r)\right] \mathrm{d}r, \tag{39}$$

and

$$V = \pi \int_0^L h(r) \cdot \mathrm{d}(r^2) \tag{40}$$

$$= \pi \int_0^R h(r) \cdot \Theta\left[h(r)\right] \mathrm{d}(r^2), \tag{41}$$

in which the theta function is approximated by a logistic function while the integral is computed by trapezoidal rule.

S5.2. The AMOC model

When the circulation changes direction, the advection term undergoes some permutations (Scott et al., 1999). To use implicit time stepping, we need to smoothen this transition. In line with (Titz et al., 2002), we define q_+ and q_- as

$$q_+ = \frac{q}{1 - e^{-kq}}, \tag{42}$$

$$q_- = \frac{q}{1 - e^{kq}}, \tag{43}$$

with k the fitting parameter, a non physical constant here set to 200. We can then replace the advection term using those two contributions. For example, equation 12 becomes

$$\dot{T}_1 = q_+ (T_2 - T_1) + q_- (T_1 - T_3) + \lambda(\tau_1 - T_1). \tag{44}$$

S5.3. The WAIS model

Our numerical scheme follows the approach in (Mulder et al., 2018) without change.

References

Benn, D. I., Hulton, N. R., & Mottram, R. H. (2007). 'calving laws', 'sliding laws' and the stability of tidewater glaciers. *Annals of Glaciology*, *46*, 123–130. doi: 10.3189/172756407782871161

Bueler, E., Lingle, C. S., Kallen-Brown, J. A., Covey, D. N., & Bowman, L. N. (2005). Exact solutions and verification of numerical models for isothermal ice sheets. *Journal of Glaciology*, *51*(173), 291–306. doi: 10.3189/172756505781829449

Glorot, X., Bordes, A., & Bengio, Y. (2011). Deep sparse rectifier neural networks. In *Proceedings of the fourteenth international conference on artificial intelligence and statistics* (Vol. 15, pp. 315–323). Fort Lauderdale, FL, USA: Proceedings of Machine

Learning Research.

Greve, R., & Blatter, H. (2009). *Dynamics of ice sheets and glaciers*. Berlin, Germany: Springer.

Lucarini, V., & Stone, P. H. (2005). Thermohaline circulation stability: a box model study. Part I: uncoupled model. *Journal of Climate*, *18*(4), 501 - 513. doi: 10.1175/JCLI-3278.1

McCarthy, G. D., Smeed, D. A., Johns, W. E., Frajka-Williams, E., Moat, B. I., Rayner, D., ... Bryden, H. L. (2015). Measuring the Atlantic Meridional Overturning Circulation at 26°N. *Progress in Oceanography*, *103*, 91–111.

Morlighem, M., Rignot, E., Binder, T., Blankenship, D., Drews, R., Eagles, G., ... Young, D. (2020). Deep glacial troughs and stabilizing ridges unveiled beneath the margins of the Antarctic ice sheet. *Nature Geoscience*, *13*, 1-6. doi: 10.1038/s41561-019-0510-8

Morlighem, M., Williams, C. N., Rignot, E., An, L., Arndt, J. E., Bamber, J. L., ... Zinglersen, K. B. (2017). BedMachine v3: Complete bed topography and ocean bathymetry mapping of Greenland from multibeam echo sounding combined with mass conservation. *Geophysical Research Letters*, *44*(21), 11,051-11,061. doi: https://doi.org/10.1002/2017GL074954

Mulder, T. E., Baars, S., Wubs, F. W., & Dijkstra, H. A. (2018). Stochastic marine ice sheet variability. *Journal of Fluid Mechanics*, *843*, 748–777. doi: 10.1017/jfm.2018.148

Rignot, E., Mouginot, J., Scheuchl, B., van den Broeke, M. R., van Wessem, M., &

Morlighem, M. (2019). Four decades of Antarctic Ice Sheet mass balance from 1979–2017. *Proceedings of the National Academy of Sciences of the United States of America*, *116*, 1095 - 1103.

Rooth, C. (1982). Hydrology and ocean circulation. *Progress in Oceanography*, *11*(2), 131-149. doi: https://doi.org/10.1016/0079-6611(82)90006-4

Schoof, C. (2007). Ice sheet grounding line dynamics: Steady states, stability, and hysteresis. *Journal of Geophysical Research*, *112*, F03S28. doi: 10.1029/2006JF000664

Schoof, C., & Hewitt, I. (2013). Ice-sheet dynamics. *Annual Review of Fluid Mechanics*, *45*(1), 217-239. doi: 10.1146/annurev-fluid-011212-140632

Scott, J. R., Marotzke, J., & Stone, P. H. (1999). Interhemispheric thermohaline circulation in a coupled box model. *Journal of Physical Oceanography*, *29*(3), 351 - 365. doi: 10.1175/1520-0485(1999)029⟨0351:ITCIAC⟩2.0.CO;2

The IMBIE Team. (2018). Mass balance of the Antarctic Ice Sheet from 1992 to 2017. *Nature*, *558*, 219-222. doi: 10.1038/s41586-018-0179-y

The IMBIE Team. (2020). Mass balance of the Greenland Ice Sheet from 1992 to 2018. *Nature*, *579*, 233–239. doi: 10.1038/s41586-019-1855-2

Titz, S., Kuhlbrodt, T., Rahmstorf, S., & Feudel, U. (2002). On freshwater-dependent bifurcations in box models of the interhemispheric thermohaline circulation. *Tellus A: Dynamic Meteorology and Oceanography*, *54*(1), 89-98. doi: 10.3402/tellusa.v54i1.12126

Van Den Berg, J., Van De Wal, R., & Oerlemans, J. (2006). Effects of spatial discretization in ice-sheet modelling using the shallow-ice approximation. *Journal of*

Glaciology, *52*(176), 89–98. doi: 10.3189/172756506781828935

Table S1. Parameters involved each model.

Model	Quantity	Symbol	Value
	Gravitational acceleration	g	$9.81 \cdot 10^6$ m s^{-2}
	Ice density	ρ_I	910 kg m^{-3}
	(Reference) water density	ρ_w	1000 kg m^{-3}
	Glenn exponent	n	3
GIS	Ice viscosity parameter	A	$3.17 \cdot 10^{-24}$ Pa^{-3} s^{-1}
	Melting gradient	m	0.005 years^{-1}
	Present-day temperature anomaly	$\Delta\tau_{N,IG}$	0 °C
	Present-day Snowfall rate	P_{IG}	0.3 m years^{-1}
	Present-day equilibrium line altitude	$h_{el,IG}$	1100 m
	Glacial temperature anomaly	$\Delta\tau_{N,G}$	-10 °C
	Glacial Snowfall rate	P_G	0.15 m years^{-1}
	Glacial equilibrium line altitude	$h_{el,G}$	100 m
AMOC	Mass of the polar boxes	M	$1.08 \cdot 10^{20}$ kg
	Box volume ratio	V	2
	Average salinity	S_0	35 psu
	Thermal expansion coefficient	α	$1.5 \cdot 10^{-4}$ °C^{-1}
	Haline expansion coefficient	β	$8 \cdot 10^{-4}$ psu^{-1}
	Hydraulic constant	k	$1.5 \cdot 10^{-6}$ s^{-1}
	Target temperature (box 1)	τ_1	0 °C
	Target temperature (box 2)	τ_2	30 °C
	Target temperature (box 3)	τ_3	0 °C
	Newtonian relaxation constant	λ	$1.29 \cdot 10^{-9}$ s^{-1}
WAIS	Surface mass balance	a	0.3 m years^{-1}
	Frictional constant	C	$7.62 \cdot 10^6$ Pa m$^{-\frac{1}{3}}$ s$^{\frac{1}{3}}$
	Sliding law exponent	m	1/3

Table S2. Relevant quantities defining the initial state. Quantities marked with an asterisk are tuned degrees of freedom.

Model	Quantity	Symbol	Initial state
GIS	Bedrock radius*	R	682 km
	Volume	V_N^0	$2.99 \cdot 10^6$ km^3
	Total meltwater flux	F_N^0	$1.27 \cdot 10^{-2}$ Sv
AMOC	Strength	q^0	15.9 Sv
	Precipitation in box 1	F_1^0	0.40 Sv
	Precipitation in box 3	F_3^0	0.28 Sv
WAIS	Fraction parameter	f	0.27
	Zonal extension*	y_0	358 km
	Depth integrated viscosity parameter*	$\bar{A}^0$	$2 \cdot 10^{-25}$ Pa^{-3}s^{-1}
	Volume	V_S^0	$3.39 \cdot 10^6$ km^3
	Total meltwater flux	F_S^0/f	$0.85 \cdot 10^{-2}$ Sv

Figure S1. Range over which the critical value of global warming leading to AMOC tipping $\Delta\tau_{G,c}$ varies as the coupling c_s ranges from 0 to 1, depending on the fraction f of the outflux from WAIS reaching the Southern Atlantic Ocean. The vertical line lies at our estimation $f = 0.27$.

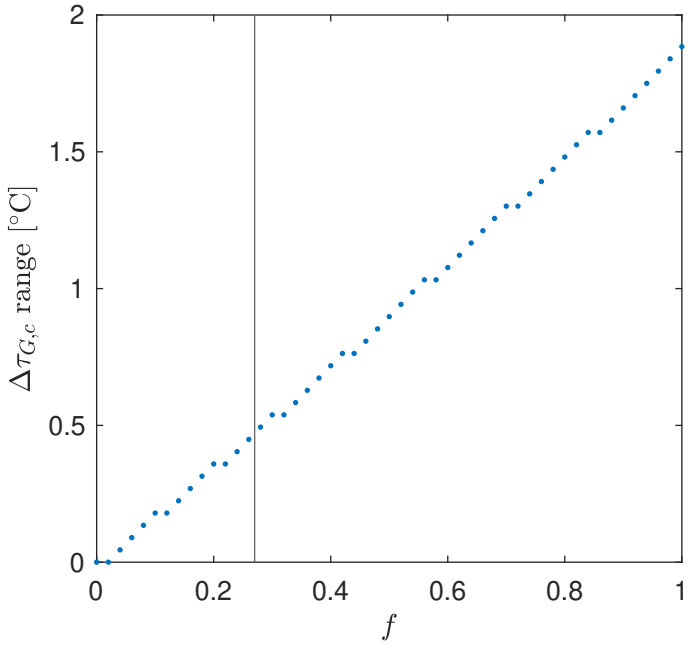

Figure S2. Transient behavior of the coupled model in hosing experiments. We represent GIS and WAIS meltwater fluxes in regimes where the AMOC does not tip (a,c) or tips (b,d). Each graph corresponds to different values of the parameter vector $(c_S, \Delta t)$: (a) $(0.25, -600)$, (b) $(0.75, -600)$, (c) $(0.75, 100)$ and (d) $(0.25, 100)$, marked as red crosses on Fig. 3.b.